Frontiers in Heat and Mass Transfer (FHMT), 8, 16 (2017)
DOI: 10.5098/hmt.8.16

Global Digital Central
ISSN: 2151-8629

Frontiers in Heat and Mass Transfer

Available at www.ThermalFluidsCentral.org

CONVECTIVE HEAT TRANSFER OF ONE ROW ARRANGEMENT OF ELLIPTICAL CYLINDER

Kaprawi Sahim*, Dewi Puspitasari†

Department of Mechanical Engineering, Sriwijaya University, Inderalaya 30662, Indonesia

ABSTRACT

One row of heated elliptical cylinder with aspect ratio 0.6 and 0.8 are studied to know the forced heat transfer performance. The transversal distance between the cylinders are changed and the heat transfer is observed. Numerical observation of the study is done by using finite volume method to solve the momentum equations in two dimension domains. The pressure term instead of velocity is obtained by measurement in a subsonic wind tunnel and then it is injected into the momentum equation. The results of the hydrodynamic calculation are then injected into the energy equation which is solved by the over relaxation iteration method. The results of numerical calculation show that the drag coefficient due to flow friction changes with the distance between two elliptic cylinders. At certain distance, the cylinders behave as single cylinder and no influence each other. The Heat transfer performance for small distance between the cylinders has lower values compared to larger distance. It increases with the increase of distances and at a certain distance, there is no more increases. It means that the heat transfer tends to a constant value. Heat transfer ability is depending on the aspect ratio of elliptic cylinder.

Keywords: *transversal distance, heat transfer, cylinder, numerical method, aspect ratio*

1. INTRODUCTION

The analytical models for the heat transfer of tube banks of in-line and staggered arrangement are developed by Khan *et al*. (2006). These models are developed in terms of longitudinal and transversal distance, Reynolds and Prandtl numbers. In this study, the authors explore the convection heat transfer associated with crossflow over the tubes for certain transverse distance. Minter Cheng (2004) gives numerical study of the influence of transverse distance from two elliptic cylinders on heat transfer. Equations of momentum in x and y directions are solved by finite volume method. In this case the pressure distribution is guessed and then it is corrected until all variables converge. The Heat transfer increase with dimensionless transverse distance ranging from 1 to 1.5 and it decreases with transversal distance from the distance greater than 1.5. The heat transfer equals to that of single cylinder if transverse distance equal to 2. Heat transfer of each row of the heat exchanger is not the same, the smallest value is found in the first row and it increases from second and third row as shown experimentally by Mehrabian (2007).

A study concerning with complex flows and heat transfer of the laminar flow regime around a single row of tubes in a channel is given by Cho J. and Son C. (2009). The time-dependent numerical approach predicted the generation and evolution of vortical structures, wakes interactions, and their effects on the drag, lift and heat transfer of the range of Reynolds number 20 to 180. Most heat transfer of flow around an elliptic cylinder occurs to the zone between stagnation point and separation point (Khan et *al*. 2005). Local variations in heat transfer are presented over the entire cylinder surface, including the zone beyond the separation points. At low Reynolds Numbers, the heat transfer of the rear portion of a tube is at a minimum values (Nakamura et *al*.,2004; A.M. Abdel-Raouf et *al*.,2010; Buyruk, 2002; Kaptan et *al*.,2008, and R. Rahman et *al*, 2005). The effects of longitudinal and transverse transversal distance on heat transfer from both arrangements are studied by Khan et *al*. (2006). They show that in both arrangements, the heat transfer increases mainly with decreasing longitudinal pith ratio, and to a lesser extent with increasing transversal distance. A laminar boundary layer develops from the front stagnation point of a cylinder in cross-flow and grows in thickness around the tube. The distributions of local heat transfer coefficients around cylinders are almost the same, except for the front half of the first row (Wang et *al*, 2000; Tahsee et *al*, 2013). Transient numerical simulations of heat transfer are performed by Andrej Horvat and Andrej at *al*. (2006) for heat exchanger segments with cylindrical and ellipsoidal tubes in the staggered arrangement. The drag coefficient and the Stanton number are lower for the ellipsoidal form in comparison to the cylindrical form of tube cross section.

It is well established that an effect of transverse distance from tubes bundles has important role in heat transfer, however, not work has been reported on the optimum limit of transverse distance especially in single row of elliptic cylinder. The purpose of this study is to investigate the optimum limit of transversal distance from hydrodynamic characteristics and heat transfer performance for one row elliptic cylinder.

2. GOVERNING EQUATIONS

Figure 1 shows the coordinate system, and parameters of this study. As shown in the figure, one row of two isothermal heated elliptic cylinders is place in a uniform stream flow. The x axis is in longitudinal direction of flow and the y axis is in direction normal to the cylinder surface. ST is the length of distance between two cylinders. The point of $\theta = 0^o$ is the point of stagnation on surface of cylinder.

* *Corresponding author. Email: kaprawi@unsri.ac.id*
† Currently in Mechanical Engineering Department, Sriwijaya University, Inderalaya, South Sumatera, 30662, Indonesia

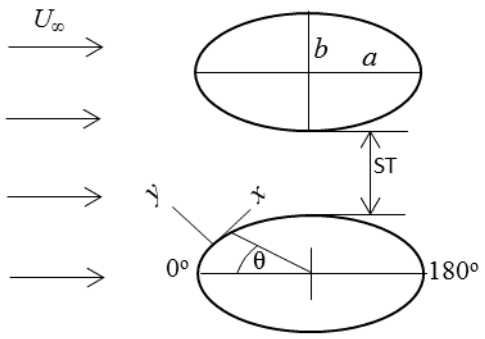

Fig. 1 Single row of elliptic cylinder

The governing continuity, momentum, and energy equations in x-direction for steady incompressible flow of a Newtonian fluid with constant thermos-physical properties, no heat generation, and negligible viscous dissipation are

Continuity equation:

$$\frac{\partial u}{\partial x}+\frac{\partial v}{\partial y}=0 \tag{1}$$

Momentum equation:

$$u\frac{\partial u}{\partial x}+v\frac{\partial u}{\partial y}=-\frac{1}{\rho}\frac{dp}{dx}+\upsilon\frac{\partial^2 u}{\partial y^2} \tag{2}$$

Energy equation:

$$u\frac{\partial T}{\partial x}+v\frac{\partial T}{\partial y}=\lambda\frac{\partial^2 T}{\partial y^2} \tag{3}$$

with boundary conditions as follows

$u = v = 0$, $T = T_S$ at the cylinder surface
$u = U_e$, $T = T_\infty$ far from cylinder

The dimensionless variables:

$$y^+=\frac{y}{L}\sqrt{R_e}\,,\quad u^+=\frac{u}{U_\infty},\quad R_e=\frac{U_\infty L}{\upsilon}\,,\ x^+=\frac{x}{L},$$

$$v^+=\frac{v}{U_\infty}\sqrt{R_e}\,,\quad {U_e}^+=\frac{U_e}{U_\infty},\quad T^+=\frac{T-T_\infty}{T_S-T_\infty} \tag{4}$$

By introducing the dimensionless variables, the equations (1), (2) and (3) become

$$\frac{\partial u^+}{\partial x^+}+\frac{\partial v^+}{\partial y^+}=0 \tag{5}$$

$$u^+\frac{\partial u^+}{\partial x^+}+v^+\frac{\partial u^+}{\partial y^+}={U_e}^+\frac{d{U_e}^+}{dx^+}+\frac{\partial^2 u^+}{\partial {y^+}^2} \tag{6}$$

$$u^+\frac{\partial T^+}{\partial x^+}+v^+\frac{\partial T^+}{\partial y^+}=\frac{1}{\mathrm{Pr}}\frac{\partial^2 T^+}{\partial {y^+}^2} \tag{7}$$

and the boundary condition become

$u^+ = v^+ = 0$, $T^+ = 1$ at the cylinder surface
$u+ = {U_e}^+$, $T^+ = 0$ far from cylinder

3. METHOD OF SOLUTION

We use the finite volume method to solve the equation (4) and (5). This method is integrating the equation (5) and (6) on a small element. (Cousteix, 1980). The discretization indexes in x and y direction is represented by subscript i and j respectively. The number of nodes is 90 in x direction and the number of nodes increases to y direction as x increases where it is 140 nodes near the rear of cylinder. The calculation of velocity is carried out along the zone of boundary layer that develops on the surface of semi-elliptic cylinder from stagnation point until rear part of cylinder. The above hydrodynamic equations eq. 5 and 6 can be expressed as a general expression below

$$\frac{\partial}{\partial x^+}\left(\phi u^+\right)+\frac{\partial}{\partial y^+}\left(\phi v^+\right)=S+\frac{\partial}{\partial y^+}\left(N\frac{\partial \phi}{\partial y^+}\right) \tag{8}$$

where ϕ is the dependent variable, N is the diffusion, and S is the source term.

After integrating the equation (8) in a small element V in discretization and we obtain the following expression (Cousteix, 1980) :

$$\int_{y_i}^{y_s}\left[\phi u^+\right]_{x_n}^{x_{n+1}}dy^+ + \int_{x_n}^{x_{n+1}}\left[\phi v^+\right]_{y_i}^{y_s}dx^+ = \iint_V S.dx^+dy^+ + \int_{x_n}^{x_{n+1}}\left[N\frac{\partial u}{\partial y}\right]_{y_i}^{y_s}dx^+ \tag{9}$$

After evaluating the integration of equation (9), the discretized equation is obtained. This equation forms a tridiagonal matrix that can be solved easily by the Cholesky method to obtain the velocity distribution in hydrodynamic boundary layer. The first term of the right hand of equation (6) is obtained by the measurement the static pressure in wind tunnel with test section of 40 x 40 cm^2 and length 100 cm. Two elliptic cylinders with aspect ratio of $\varepsilon = 2b/2a = 0.6$ and 0.8 are placed as the arrangement shown by Fig. 1. The static pressures are measured at the surface of cylinder from $\theta = 0^o$ to 180^o. The calculation of Reynolds number is based on the measured maximum velocity between the cylinders. After calculation, we obtain maximum velocity $U_{\max} = 15$ m/s for the cylinders with the smallest transverse distance and the Reynolds number is 8.4×10^4 which is laminar flow and it is less than the value of the transition Reynolds number (John et *al*. 2008).

The solution to the energy equation (7) is carried out with iteration method. The equation is discretized with finite difference method to obtain the discretized equation and then it is easily solved by the iteration method using factor of relaxation. The number of nodes of x and y direction in the calculation of the temperature is equal to the number of nodes in velocity calculation. We use the backward and centered difference in the left side of the equation (7). After transformation process, equation (7) becomes the discretized equation as follows.

$$u_{i,j}^+\left(\frac{T_{i,j}^+-T_{i-1,j}^+}{\Delta x^+}\right)+v_{i,j}^+\left(\frac{T_{i,j+1}^+-T_{i,j-1}^+}{2\Delta y^+}\right)=\frac{1}{\mathrm{Pr}}\left(\frac{T_{i,j+1}^+-2T_{i,j}^++T_{i,j-1}^+}{\Delta {y^+}^2}\right) \tag{10}$$

Global Digital Central
ISSN: 2151-8629

The velocity distribution in equation (10) are known from previous calculation (eq. 9). We use Pr = 0.71 for air and for all calculation in this study.

The pressure drag coefficient is calculated from the common equation as follows

$$Cp = \frac{p_i - p_\infty}{1/2.\rho U_\infty^2} \tag{11}$$

The skin friction drag is calculated starting from stagnation point to point of separation. The drag coefficient is given by

$$C_{DF} = \frac{2.\int_0^\pi \tau_w \sin\alpha.dA}{\frac{1}{2}.\rho U_\infty^2 A}$$

or using the variables in equation (4), the drag coefficient due friction becomes

$$C_{DF}.\mathrm{Re}^{1/2} = 4.\int_0^{x_s^+} \left.\frac{\partial u^+}{\partial y^+}\right|_{y^+=0} \sin\alpha.dx^+ \tag{12}$$

and the average Nusselt number is written

$$Nu/\mathrm{Re}^{1/2} = \frac{1}{x^+}\int_0^{x_s^+} \left.\frac{\partial T^+}{\partial y^+}\right|_{y=0} dx^+ \tag{13}$$

4. RESULTS AND DISCUSSION

The solution of the energy equation by using the iteration method need the factor of relaxation of 0.5 and the number of iteration is about 700. The temperature variables at of all nodes converge to the solution where the absolute convergence are less than 10^{-6}. The calculation of all parameters is carried out from stagnation point to the separation point of flow. The coefficients of pressure are presented in Fig. 2 and 3 for ε = 0.6 and 0.8 respectively. The dimensionless transversal distance is represented by $ST^+ = ST/2b$ in which $2b$ is minor axis of elliptic cylinder (Fig.1). In pressure measurements, the distance between cylinders ST is set at constant values for all aspect ratio of elliptic cylinders, while the length of minor axis is different. It is the reason that the values of ST^+ are quite different for two type of elliptic cylinder. It is noted that the length of minor axis increases when the aspect ratio increases and, vice versa, the length of minor axis decreases when the aspect ratio decreases. That is why, ST^+ has different values for ε = 0.6 and 0.8 as shown in Fig. 2 and 3 where. ST^+ has higher values for ε = 0.6.

Figures 2 and 3 show that for small distance between cylinders, the pressure decrease to the lowest values compared to the other distances. The region near the stagnation point, the pressure seems constant to the certain distance compared to the pressure of other cylinder in the same areas. This leads to constant velocity due to small areas passes between cylinders. When the distances increase, the pressure coefficient slightly difference in values and its similar. The elliptic cylinder with aspect ratio ε = 0.6, the pressure at the rear region of cylinders are greater than that of cylinder with aspect ratio of 0.8 (Fig.3) since the pressure coefficient Cp is about -1.5 for ε = 0.6 while the Cp is about -2.0 for ε = 0.8. As shown by the equation (11) that the pressure parameter p_i changes along the surface of cylinder while the others parameters are constant values. The lower aspect ratio of elliptic cylinder tends to have streamline flow at the rear region, but the higher aspect ratio tends to increase the wake region at the rear part so the pressure decreases. The higher value of aspect ratio makes the wake region of rear cylinder higher so the pressure decreases. The other observation is near stagnation point, in which the pressure for ε = 0.6 decrease rapidly compared to the cylinder of ε = 0.8. $ST^+ \approx 0.11$ for both ε = 0.6 and 0.8 on the rear part of cylinder, the pressure decreases far from the the others values of $ST^+ > 1.1$ since the flow between cylinder becomes a jet flow which induces high pressure decrease.

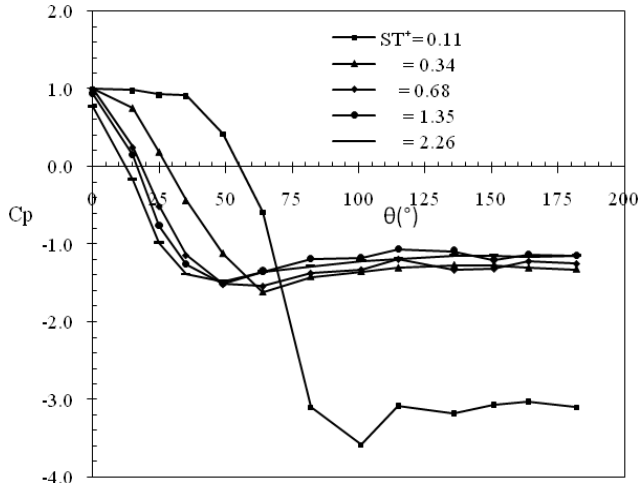

Fig. 2 Pressure Coefficient for ε = 0.6

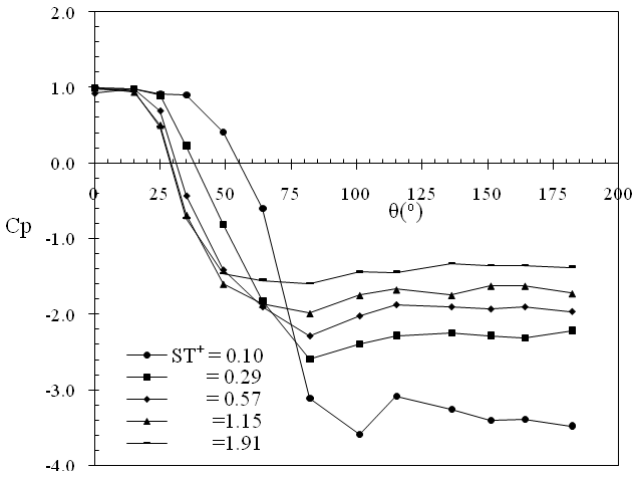

Fig. 3 Pressure Coefficient for ε = 0.8

The pressure coefficient leads to have the total drag coefficient due to static pressure as shown by Fig. 4. The distance between cylinders may not be zero in order to have fluid flows. Therefore, the curves start from small distances. It is clear that the drag coefficient profile is different to significant values of all aspect ratios. For all aspect ratios of cylinder, the maximum values are observed when the distances are small and its decrease to the minimum values for large distance. It is clear that the total drag coefficient is larger for ε = 0.8 compared with that of coefficient for ε = 0.6 in all ST^+. For ε = 0.6, the coefficient decreases significantly starting from about $ST^+ \approx 0.6$. After this value, the coefficient decreases slowly and the influence may be neglected. So the elliptic cylinders behave as a single cylinder, practically, there is no influence of each other. For ε = 0.8, the coefficient decreases with ST^+ more rapidly compared with that of ε = 0.6. Small distance leads to small frontal area between cylinders, so the fluid accelerates and the pressure drops.

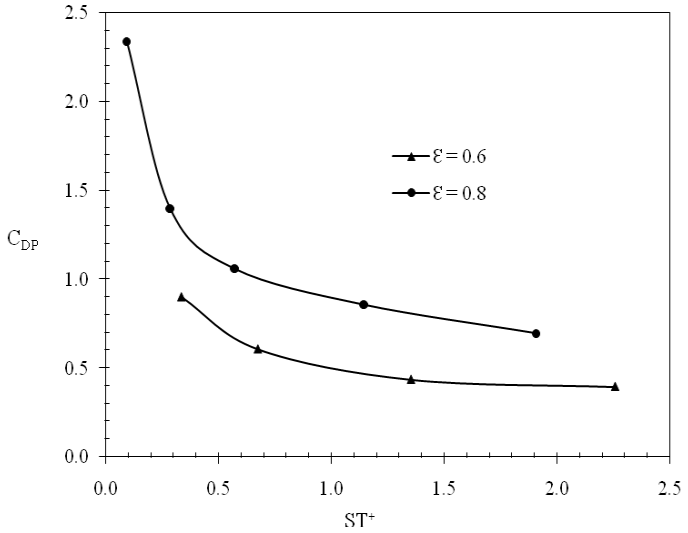

Fig. 4 Pressure Drag Coefficient

The velocity distributions in the boundary layer produce the drag coefficient due to friction. The friction drag coefficient of two types of elliptic cylinder is shown by Fig. 5. $C_{DF}.Re^{1/2}$ represents the parameter of dimensionless shear stress at the surface of cylinder as shown by equation (12) which relates to the velocity gradient at the wall. Furthermore, this parameter represents the velocity at the position very close to the surface of cylinder. For ε = 0.6, the drag coefficient profile is smaller than that for ε = 0.8. It is clear from the figure that the coefficient decreases with increasing ST^+. The increase in ST^+ makes the flow area between cylinders increases that causes the decrease of velocity.

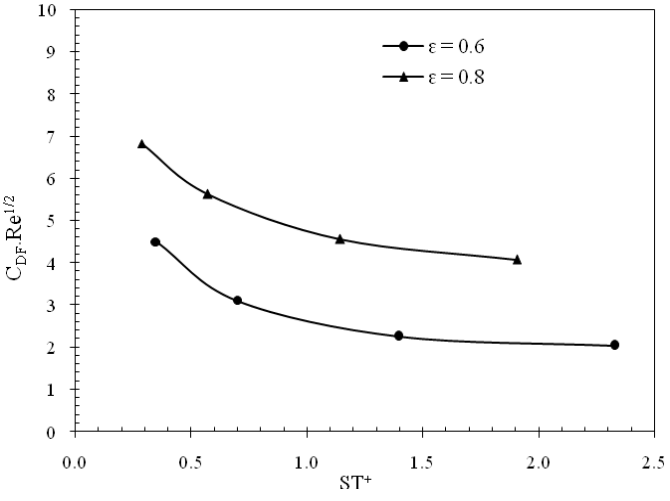

Fig. 5 Friction Drag Coefficient

For brevity, the complete results of temperature distribution are not presented here. Two examples of the dimensionless temperature profile distributions are presented by Fig. 6 and 7 for certain ST^+ and for some angle θ. The figures show the fluid temperatures in direction normal to the cylinder surface and have similar trends. The dimensionless temperature at the cylinder surface ($y^* = 0$) for all aspect ratios is equal to unity and temperature toward zero far from the surface since the boundary condition is imposed on the solution to the equation (7). In this case, the convection occurs starting from the cylinder surface to the fluid or the surface temperature is greater than the fluid temperature. The elliptic cylinder with ε = 0.6 shows that the curves are practically coinciding for θ ≤ 30.5°. It means that the temperature distributions of front region of cylinder are practically the same each other. The same case for ε = 0.8, the curves are coinciding each other in wide region of about θ ≤ 76.1°. For all cases, from the surface, the curves seem to decrease linearly with y^* to at a certain value and then reach to zero asymptotically far from the surface. In case of larger θ, the temperature profiles have the difference distribution of that of smaller θ, but still similar. The temperatures distribution has greater than that of smaller θ since the thermal boundary layer develops starting from point of stagnation to near point of separation. As θ increases, the temperature profiles differ from that for small θ. In this case, the temperature distributions are larger than for small angle. The increase in temperature is caused by the decrease in thermal boundary layer thickness. Thus for ε = 0.6, the thermal boundary layer develops more rapidly than for ε = 0.8.

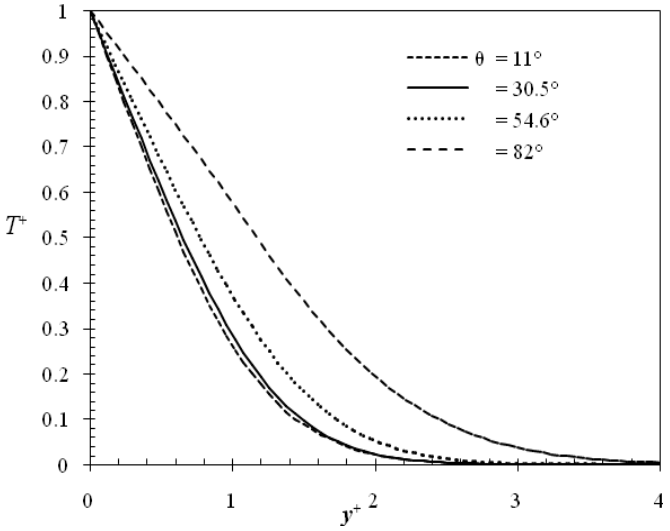

Fig. 6 Temperature Profile for ε = 0.6 and ST^+ = 0.67

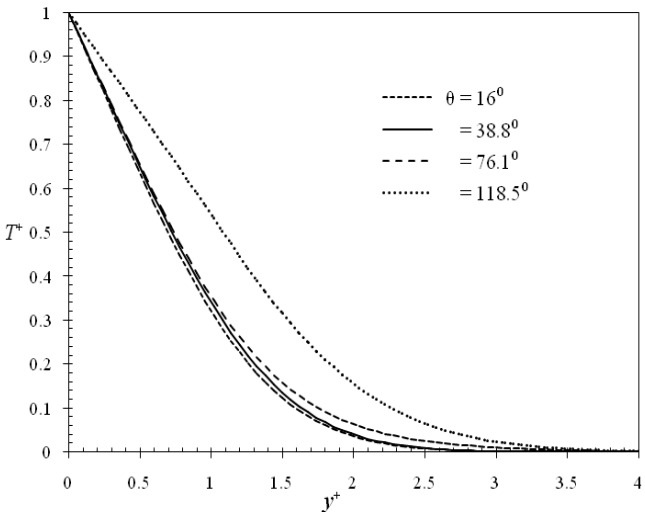

Fig. 7 Temperature Profile for ε = 0.8 and ST^+ = 0.5

Figure 8 compares the local heat transfers for different distances ST^+ and for ε = 0.6. It seems that the results are strongly influenced by the nature of transversal distances small distance ST^+ <1.35 since the curves seem to be coincided each other after $ST^+ \geq 1.35$. For higher ST^+ there is no influence on heat transfer performance. It can be also observed that for small transverse distance, the heat transfer performance profile is lower than that of larger distance. However, for all $ST^{+,}$ starting at the maximum values of $Nu/Re^{1/2}$ at stagnation point

$\theta = 0^o$, $Nu/Re^{1/2}$ decreases with increasing of θ as a result of laminar boundary layer development. The minimum heat transfer is reached near the separation point. The decrease in $Nu/Re^{1/2}$ is due to a corresponding increase in hydrodynamic boundary layer thickness. The cross section of flow produced by two elliptic cylinders with $\varepsilon = 0.6$ decreases gradually which make the variation on flow behavior. The flow accelerates with decrease of cross section which produces the decrease of pressure and after passing the minimum cross section the velocity is at maximum. At the rear region of cylinder, the flow decelerates and the pressure re-increases. Thus the boundary layer develops starting from stagnation point where the cross section is maximum.

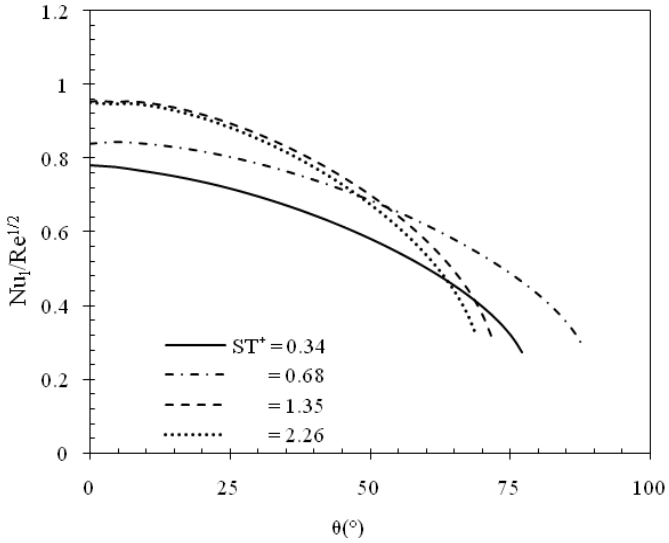

Fig. 8 Local Nusselt Number for $\varepsilon = 0.6$

The important difference is observed between $\varepsilon = 0.6$ and $\varepsilon = 0.8$. of local heat transfer profile. Fig. 9 shows the parabolic profile of local heat transfer, particularly for $ST^+ = 0.28$. So for very small distance, the local heat transfer increases with θ from stagnation point. It reaches a maximum at $\theta \approx 75^o$ and then decreases to the minimum value near separation point. A maximum value is due to the temperature deformation in *x* direction and thus the temperature gradient becomes important which makes the highest Nusselt number parameter. $ST^+ = 0.28$, the narrow spacing between cylinder influences boundary layer which makes the flow becomes a jet flow thus decreasing the boundary layer thickness. Thus the local heat transfer is more sensitive to the local heat transfer profile in small distance. The curve distributions of $ST^+ > 0.28$ show similar profiles but we observe small differences in about $\theta \leq 60^o$. In this region, the higher ST^+ and the higher heat rate transfer and the local heat transfers increase slightly with increase of θ to a maximum value of $\theta \approx 40^o$, then it decrease rapidly toward the separation points. This provides further evidence that temperature interference is almost negligible and the similarity of the temperature profile of each ST^+ is kept. There is almost no effect on the heat transfer characteristics of elliptic cylinders. Further, it is observed for $\theta \geq 60^o$, the heat transfer parameter curves shift to the left part of the figure keeping its similarity by the increase of ST^+. The heat transfer rate is sensitive to the variation in the rear part of the elliptic cylinder especially for narrow distance where the $Nu_l/Re^{1/2}$ decrease rapidly approaches the separation point. This condition is due to the thinness of thermal boundary layer at the rear part of cylinder.

The heat transfer ability is represented by the average Nusselt number parameter $Nu_a/Re^{1/2}$ as shown by Fig. 10. It can be seen that the heat transfer is better for $\varepsilon = 0.6$ in range of about $ST^+ \geq 0.8$, but for lower ST^+, the heat transfer is lower than that of cylinder with $\varepsilon = 0.8$. The significant increase in heat transfers is observed in the range of about $0.34 < ST^+ < 1.35$, while for $\varepsilon = 0.8$ the increase in heat transfers is small in the range of about $0.28 < ST^+ < 1$. That is why the two curves are intersecting at $ST^+ \approx 0.8$ which both elliptic cylinders have the same heat transfer ability. For $\varepsilon = 0.6$ and starting from $ST^+ \geq 1.35$, there is no effect on heat transfer since the curve seems to have very small variations. In case of elliptic cylinder with $\varepsilon = 0.8$, the influence seems to be important for about $ST^+ \leq 1.0$ but if the transversal distances are greater than 1.0, the effect can be neglected and the elliptic cylinder is considered as single cylinder.

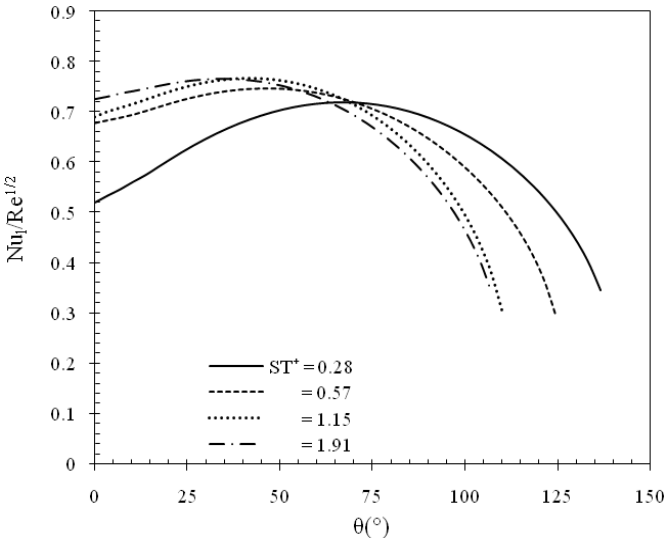

Fig. 9 Local Nusselt Number for $\varepsilon = 0.8$

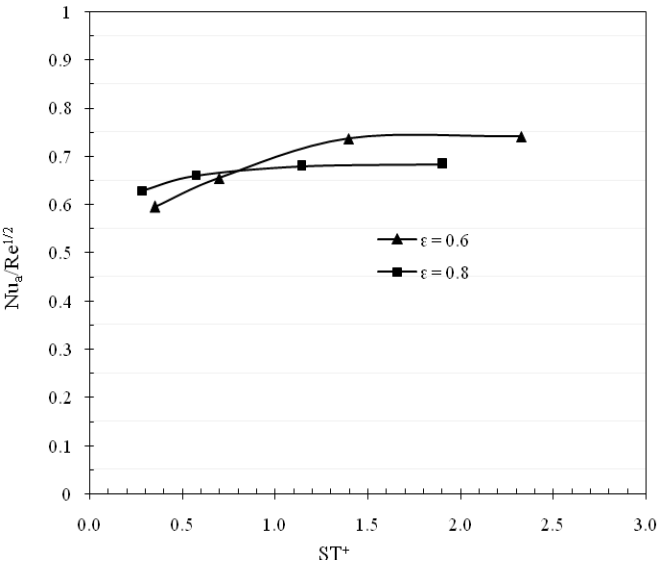

Fig. 10 Average Nusselt Number

5. CONCLUSION

Two elliptical cylinders arranged side by side are studied its heat transfer performance in which each cylinder has aspect ratio of $\varepsilon = 0.6$ and the other study has the aspect ratio of $\varepsilon = 0.8$. Study shows that the transversal distance between two elliptic cylinders have influence on hydrodynamic and thermal parameter. The influence is mostly significant for small distance, however, it depends on the aspect ratio of the elliptic cylinder. In hydrodynamic condition, the elliptic cylinder with $\varepsilon = 0.6$ has lower friction and lower pressure drag compared with

cylinder with ε = 0.8. In heat transfer condition, the elliptic cylinder with aspect ratio 0.6 has better heat transfer performance starting from $ST^+ \approx 0.8$ compared with the cylinder of aspect ratio 0.8. This study gives the limit of utilization of the elliptic cylinder in heat exchanger design.

NOMENCLATURE

a	semimajor axis of elliptic cylinder (m)
b	semiminor axis of elliptic cylinder (m)
C_{DP}	pressure drag coefficient
C_{DF}	friction drag coefficient
C_P	pressure coefficient
L	characteristic length = $2a$ (m)
Nu	Nusselt number
p	static pressure (kg/cm^2)
Pr	Prandtl number
Re	Reynolds number
ST	transversal distance between cylinder (m)
T_s	surface temperature (°C)
T_∞	upstream temperature (°C)
u	velocity in boundary layer in x direction (m/s)
U_e	velocity at boundary layer (m/s)
U_∞	upstream velocity (m/s)
v	velocity in in boundary layer in y direction (m/s)
x	coordinate (m)
y	axis (m)

Greek Symbols

υ	cinematic viscosity of fluid (m^2/s)
ϕ	dependent variable
ε	aspect ratio = $2b/2a$
θ	angle (°)

Superscripts

+	Dimensionless parameter

Subscripts

i	discretization number in x direction
j	discretization number in y direction

REFERENCES

Abdel-Raouf A.M, M.Galal, and E.E.Khalil, 2010, "Heat Transfer past Multiple Tube Banks: A Numerical Investigation," *10th AIAA/ASME Joint Thermophysics and Heat Transfer Conference, Fluid Dynamics and Co-located Conferences*.
http://dx.doi.org/10.2514/6.2010-4769

Andrej Horvat and Borut Mavko, 2006, "Heat Transfer Conditions in Flow across a Bundle of Cylindrical and Ellipsoidal Tubes," *Numerical Heat Transfer*, Part A, **49**, 699–715.
http://dx.doi.org/10.1080/10407780500496554

Buyruk, E., 2002. "Numerical Study of Heat Transfer Characteristics on Tandem Cylinders, Inline and Staggered Tube Banks in Cross-Flow of Air," *Int. Comm. Heat Mass Transfer*, 29: 355-366.
http://dx.doi.org/10.1016/S0735-1933(02)00325-1

Cho J and Son C., 2009, "A Numerical Study of the Fluid Flow and Heat Transfer around a Single Row of Tubes in a Channel using Immerse Boundary Method," *Journal of Mechanical Science and Technology,* **22**, 1808~1820.
http://dx.doi.org/10.1007/s12206-008-0507-5

Cousteix P, 1980, "Couch Limite Laminaire," Cepadus, Paris

John H. Lienhard IV / John H. Lienhard V., 2008, *A Heat Transfer Textbook*, Third Edition.

Kaptan, Y., E. Buyruk, and A. Ecder, 2008. "Numerical Investigation of Fouling on Cross-Flow Heat Exchanger Tubes with Conjugated Heat Transfer Approach,". *Int. Comm. Heat Mass Trans*., **35**, 1153-1158.
http://dx.doi.org/10.1016/j.icheatmasstransfer.2008.05.005

Khan W.A, Culham J.R, Yovanovich M. M. 2005, "Fluid Flow Around and Heat Transfer from an Infinite Elliptic Cylinder," *Journal of Heat Transfer*, **127**(7), 785-790.
http://dx.doi.org/10.1115/1.1924629

Khan W.A, Culham J.R, Yovanovich M.M, 2006, "Convection Heat Transfer from Tube Banks in Crossflow: Analytical approach," *International Journal of Heat and Mass Transfer,* **49**, 4831–4838.
http://dx.doi.org/10.1016/j.ijheatmasstransfer.2006.05.042

Nakamura, H. & Igarashi, T., 2004, "Unsteady Heat Transfer from an Elliptic Cylinder for Reynolds Numbers from 3000 to 15,000," *International J. of Heat and Fluid Flow*, **25**, 741–748.
http://dx.doi.org/10.1016/j.ijheatfluidflow.2004.05.012

Mehrabian, M. A. 2007, "Heat Transfer and Pressure Drop Characteristics of Cross Flow of Air over an Circular Tube in Isolation and/or In a Tube Bank," *The Arabian Journal for Science and Engineering*, Vol. 32, Issue 2B

Minter Cheng, 2004, "Fluid Flow and Heat Transfer Around Two Elliptic Cylinders in Side-By-Side Arrangement," *Proceedings of HT-FED04 2004 ASME Heat Transfer/Fluids*. Engineering Summer Conference, July 11-15, Charlotte, North Carolina, USA

Rahmani R., I. Mirzaee, and H Shirvani, 2005, "Computation of a Laminar Flow and Heat Transfer of Air for Staggered Tube Arrays in Cross-flow," *Iranian Journal of Mechanical Engineering* Vol. 6, No. 2.

Wang Yan-Xing, Zhao Hong, Lu Xi-Yun, Zhuang Li-Xian, 2000, "Finite Element Analysis of Laminar Flow and Heat Transfer in a Bundle of Cylinders," *Journal of Hydrodynamics*, Ser B, 4, 99- 108

Tahsee A.T.M. Ishak and M.M. Rahman, 2013, "A Numerical Study of Forced Convection of Air on for In-line Bundle of Cylinders Crossflow," *Asian Journal of Scientific Research*, **6**(2), 217-226.
http://dx.doi.org/10.3923/ajsr.2013.217.226